Colloidal ruthenium catalysts for selective quinaldine hydrogenation: Ligand and solvent effects

Vincent Colliere, Marc Verelst, Pierre Lecante, M. Rosa Axet

Chemistry–A European Journal
Research Article
doi.org/10.1002/chem.202302131
Chemistry Europe
European Chemical Societies Publishing
www.chemeurj.org

Colloidal ruthenium catalysts for selective quinaldine hydrogenation: Ligand and solvent effects

Vincent Colliere,[a] Marc Verelst,[b] Pierre Lecante,[b] and M. Rosa Axet*[a]

Colloidal Ru nanoparticles (NP) display interesting catalytic properties for the hydrogenation of (hetero)arenes as they proceed efficiently in mild reaction conditions. In this work, a series of Ru based materials was used in order to selectively hydrogenate quinaldine and assess the impact of the stabilizing agent on their catalytic performances. Ru nanoparticles stabilized with polyvinylpyrrolidone (PVP) and 1-adamantanecarboxylic acid (AdCOOH) allowed to obtain 5,6,7,8-tetrahydroquinaldine with a remarkable selectivity in mild reaction conditions by choosing the suitable solvent. The presence of a carboxylate ligand on the surface of the Ru NP led to an increase in the activity when compared to Ru/PVP catalyst. The stabilizing agent had also an impact on the selectivity, as carboxylate ligand modified catalysts promoted the selectivity towards 1,2,3,4-tetrahydroquinaldine, with bulky carboxylate displaying the highest ones.

Introduction

Selective hydrogenations of (hetero)arenes are of interest in organic synthesis and are applied on large scale for the production of fine and bulk chemicals.[1,2] Aromatic cyclic amines are of interest for several fields including pharmaceutical and fine chemicals.[3] Particularly, 1,2,3,4-tetrahydroquinolines are key intermediates in agrochemicals, pharmaceuticals and various fine chemicals.[4] Its preparation includes intramolecular cyclization reactions, Povarov reactions, rearrangement reactions, partial hydrogenation of quinolines, among others.[4] The hydrogenation of quinolines is an interesting approach as it circumvents the use of multistep procedures. Homogeneous and heterogeneous catalysts have been described for the hydrogenation of quinolines,[1,4] usually based in platinum-group metals. Heterogeneous catalysts based on Au,[5] Pt,[6] Pd,[7] Ir,[8] Rh,[9–11] Ru[12–14] are highly efficient for this reduction reaction. Earth-abundant based catalysts, such as Fe,[15] Co,[16] Ni,[17] and Mn,[18] usually needing harsher reaction conditions than catalysts based on noble metal, have been described as well for this application. The asymmetric hydrogenation of quinolines has been only achieved using homogeneous catalysts.[19] The modification of the intrinsic properties of metallic heterogeneous catalysts may be achieved using several strategies,[20] among them, the use of organic surface adsorbates is a straightforward manner to reach this desirable goal.[21] Some of us have previously shown that changing the ligand present on the metallic surfaces can modulate the catalytic properties of the nanocatalysts.[22,23] In previous works, we have demonstrated that carboxylic acid-modified ruthenium nanoparticles (NP) are electron-deficient metallic surfaces, very robust for several catalytic hydrogenation reactions,[24–26] which could be of interest for this reaction.[9,26,27] First, the optimization of the reaction conditions with well-described colloidal Ru catalysts was investigated; stabilized Ru NP with polyvinylpyrrolidone (PVP), Ru/PVP, and 1-adamantanecarboxylic acid (AdCOOH), Ru/AdCOOH, were used with this aim. The results pointing to an important effect of the solvent and the ligand in the outcome of this reaction. Then, using a chiral, bulky-modified Ru NP, Ru/(BINA(COOH)$_2$ where BINA(COOH)$_2$ is an axially chiral 1,1′-binaphthyl-2,2′-carboxylic acid, the possibility of an asymmetric induction on the hydrogenation of quinaldine was studied.

Results and Discussion

The selective hydrogenation of quinaldine (Scheme 1) was investigated using several Ru colloidal systems in order to elucidate the impact of the solvent and the ligand in the outcome of the reaction. First, previously reported catalysts, Ru/PVP[23] and Ru/AdCOOH,[24] were used with this aim. Both systems displaying an electron-deficient Ru surface as demonstrated experimentally and theoretically;[23,24,28,29] due to the presence of hydrides on the surface for Ru/PVP, and hydrides and the corresponding carboxylate AdCOO$^-$ species for Ru/AdCOOH. In a previous work by some of us,[9] we have determined that the presence of an electron-deficient ligand, fullerene C_{60}, and the hydrides on the surface of Rh NP were key parameters to promote high selectivity towards the hydrogenation of the N-bearing cycle of quinoline. Taking into

[a] V. Colliere, Dr. M. R. Axet
CNRS, LCC (Laboratoire de Chimie de Coordination), Université de Toulouse, UPS, INPT, 205 route de Narbonne, BP 44099, F-31077 Toulouse Cedex 4, France
E-mail: rosa.axet@lcc-toulouse.fr
[b] Dr. M. Verelst, Dr. P. Lecante
Centre d'Elaboration de Matériaux et d'Etudes Structurales, Université de Toulouse–UPS, 29 rue Jeanne Marvig, Cedex 4, 31055 Toulouse, BP 94347, France

Supporting information for this article is available on the WWW under https://doi.org/10.1002/chem.202302131

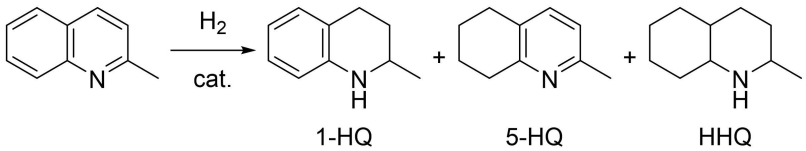

Scheme 1. Quinaldine hydrogenation.

account these premises, a series of quinaldine hydrogenation reactions were carried out using Ru/PVP and Ru/AdCOOH NP (Figure 1) in batch conditions for 24 h under 35 bar of H_2 pressure at low temperature (room temperature or 35 °C). The results are summarized in Table 1.

The solvent had a significant effect on the catalytic activity of Ru/PVP. In 1-PrOH, the reaction was almost complete after 24 h of reaction at room temperature under 35 bar of H_2 pressure, while in pentane only a slight conversion was observed after the same period of time, and, in dodecane, no activity was observed. Intermediary conversions were observed for the other solvents. Plots of activity and selectivity towards the carbocycle, 5,6,7,8-tetrahydroquinaldine (5-HQ), *vs.* several common properties of solvents[30] as well as the solubility of H_2[31] on them are depicted in the SI (Table S1, Figure S1–S2). The trends in selectivity are usually evaluated at isoconversion, lacking of these data, we assumed that selectivity towards 5-HQ remained rather constant, as it can be intuitively inferred from data on Table 1, and clearly seen in time-concentrations curves over time presented in the SI. As the catalyst was also active for the hydrogenation of toluene, the analyses were done by removing this point in the correlations. We have checked if this phenomenon is consequence of the different hydrogenation kinetics displayed by the intermediates, 1-HQ and 5-HQ, and quinaldine itself, by engaging independently 1-HQ and 5-HQ as substrates in 1-PrOH (Figure S3). In this conditions 1-HQ was not hydrogenated, thus, suggesting a poisoning of the metallic surface, similarly 5-HQ was only converted to HHQ in a 20%, indicating in turn a poisoning after some reduction. A subtle balance seems to operate in this Ru colloidal system, in general, which probably is related to the Lewis-basic properties of the compounds.[1,10,32] More analyses needs to be done to clarify this point that are beyond the scope of this work.

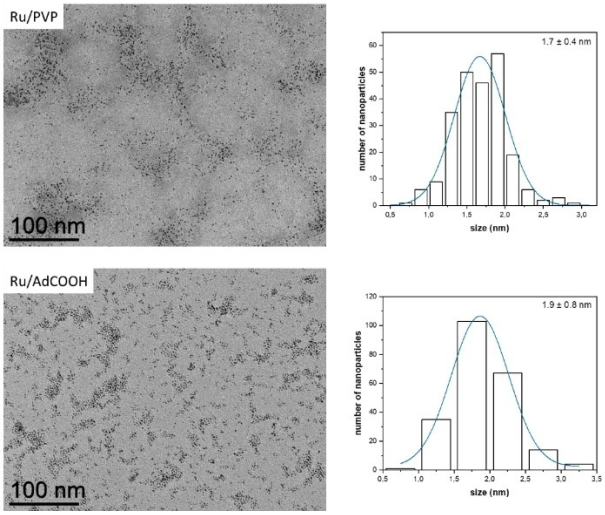

Figure 1. TEM images of Ru/PVP and Ru/AdCOOH (scale bar 100 nm) together with their respective size histogram.

Of all properties analysed, permittivity showed a good linear correlation with both activity and selectivity. In previous works, it has been calculated that in hydrogenation reactions permittivity plays a role changing thermodinamics,[33] but also the kinetics and the solvation of the chemical species involved in the hydrogenation.[34] Correlations between permittivity and selectivity have also been described experimentally.[35] In particular, for hydrogenation of quinoline solvent effects have been observed for activity, but not for selectivity, and have been directly correlated to the permittivity. The density, the boiling point, the viscosity, or the dipole moment of the solvents did not show a significant relationship with the hydrogenation reaction outcome. The hydrogen-bond acceptance of the solvent has no apparent effect on selectivity or activity either; yet, solvents with higher values promote the activity and decrease the selectivity towards the carbocycle. The solubility of H_2 in a given solvent appears to have an influence in the activity and the selectivity of the reaction. Higher solubility of H_2 leading to an enhanced hydrogenation of the carbocycle ring. Some of us have shown that the hydride coverage of the NP metallic surface plays an important role on the coordination of reactants and reagents.[9,23,27] For instance, in the hydrogenation of quinoline using Rh NP the coordination mode of quinoline was significantly affected by the hydride coverage of the metallic NP.[9] It could be plausible, thus, that hydrogen solubility have an effect on the hydride coverage, modulating the selectivity in turn, as the adsorption mode of quinaldine may be modified. The solvent effect on activity could be also due to the dispersibility of Ru/PVP on the different solvents screened, as PVP stabilized NP are known for the poor colloidal stability in low polarity solvents, as observed qualitatively here, or by others.[36] It could be also plausible that the solvent effect on selectivity could be due to a swelling or shrinking of the PVP due to the presence of the solvent. To assess some of these hypotheses, Ru/AdCOOH was used as catalyst in 1-PrOH, THF, and Et_2O using the same reaction conditions. Regarding the activity, Ru/AdCOOH was more active than Ru/PVP, (Table 1, entries 1, 3 and 7 vs. 12, 14, 16, respectively), which points out to the poor solubility of Ru/PVP in apolar solvents as a factor for the decrease of activity, yet the use of apolar solvents led to a decrease of activity for the Ru/AdCOOH series as well (Table 1, 12 to 17). Ru/AdCOOH catalyst was highly disperse in all the solvents tested indicating then

Table 1. Selective hydrogenation of quinaldine Ru/PVP and Ru/AdCOOH nanocatalysts.[a]

Entry	Solvent	T (°C)	t (h)	Conversion (%)[b]	1-HQ (%)[b]	5-HQ (%)[b]	HHQ (%)[b]
Ru/PVP							
1	1-PrOH	r.t.[c]	24	95	62	27	11
2		35	24	>99	10	29	61
3	THF	r.t.[c]	24	35	45	50	5
4		35	24	65	37	54	9
5	Toluene	r.t.[c]	24	8[d]	14	86	–
6		35	24	34[e]	23	70	7
7	Et_2O	r.t.[c]	24	12	12	86	2
8		35	24	39	9	86	4
9		50	24	58	19	72	9
10	Pentane	r.t.[c]	24	>1	14	86	–
11	Dodecane[f]	r.t.[c]	24	–	–	–	–
Ru/AdCOOH							
12	1-PrOH	r.t.[c]	24	>99	21	18	61
13		35	24	>99	–	12	88
14	THF	r.t.[c]	24	91	56	37	7
15		35	24	>99	24	32	44
16	Et_2O	r.t.[c]	24	74	25	72	3
17		35	24	>99	20	69	11
Ru/C							
18	1-PrOH	r.t.[c]	24	79	>99	–	–

[a] Reaction conditions: 1×10^{-2} mmol of metal, 1 mmol of quinaldine, 0.25 mmol of dodecane (internal standard), 35 bar of H_2, 5 mL of solvent. [b] Determined by GC using an internal standard technique. [c] Room temperature was in the range 20–23 °C. [d] 0.43 mmol of methylcyclohexane were detected in the reaction media due to the hydrogenation of the solvent (toluene). [e] 1.67 mmol of methylcyclohexane were detected in the reaction due to the hydrogenation of the solvent (toluene). [f] 0.25 mmol of decane were used as internal standard.

that solubility of the catalyst is not the only parameter governing the activity. More interesting is the effect of the solvent on the selectivity of this reaction. The trend found in Ru/PVP was also observed using Ru/AdCOOH as catalyst. In Et_2O high selectivity towards the hydrogenation of the carbocycle was found, at 35 °C full conversion was attained at 24 h (Table 1, entry 17) with an excellent selectivity towards 5-HQ of 69%. Similar correlations of selectivity/activity towards solvent properties are observed for Ru/AdCOOH catalysts (Figure S2). Although our data is narrow and probably there is a balance of several factors, it seems to emerge that polar solvents promote the hydrogenation reaction, while enhancing the selectivity towards the hydrogenation of the N-cycle, while in non-polar solvents the reaction proceeds less efficiently, but displaying a remarkable selectivity towards the carbocycle hydrogenation (> 70% at 60% of conversion for Ru/PVP and 69% at full conversion using Ru/AdCOOH). It is worth noting that high selectivity towards carbocycle hydrogenation in quinolines and other related N-heterocycles has been described for hydrogenations performed with homogeneous[37] and heterogeneous[38] catalysts; the later mainly based in Pt catalysts in acidic media. It is well documented that the hydrogenation of quinolines, isoquinolines, and their analogues occurs usually in the heteroaromatic ring; and usually this selectivity is the one observed in Ru-based heterogeneous catalysts.[12,39] Few exceptions to that have been described for Ru-based catalysts: using a Ru/hectorite catalysts, $NaBH_4$, 60 °C and a mixture of ethanol/water or dimethylformamide/water, 2-phenylquinoline was selectivety converted to 2-phenyl-5,6,7,8-tetrahydroquinoline in a 99%;[13] also, the reduction of the carbocycle of quinoline and related compounds was enhanced when adding molecular sieves to the reaction media, achieving up to 95% of selectivity in the hydrogenation of 3-methyl-quinoline in isopropanol at 50 bar of H_2 pressure and 80 °C.[40] Like in the case of the highly selective catalysts based on Pt the hydrogenation towards the carbocycle is favored[38] it is suggested by the authors that the acidic character of the molecular sieves plays an important role for that observation. It is worth noting that in our case, no additive was needed in order to achieve a remarkable high selectivity towards the hydrogenation of the carbocycle, in very mild reaction conditions.

Examples of heterogeneous asymmetric catalysts are scarce.[41] Cinchona alkaloid-modified catalysts are the most successful and studied systems able to induce high enantioselectivities; other catalytic systems such as tartaric acid-modified nickel and iron catalysts have shown to be able to induce chirality as well.[42] Producing heterogeneous catalysts able to provide chiral 1,2,3,4-tetrahydroquinolines is a highly desirable

goal, as, so far, it has only been achieved using homogeneous catalysts.[43] With the double aim to test if Ru NP chirally modified are able to induce asymmetry and also to study the role of the bulkiness of the ligand in the hydrogenation reaction of quinaldine, a set of three Ru NP nanocatalysts were synthesised: a racemic Ru/(*rac*)-BINA(COOH)$_2$, and two chiral Ru/(*R*)-BINA(COOH)$_2$, and Ru/(*S*)-BINA(COOH)$_2$, following the procedure described in Scheme 2. Details are given in the experimental part. Table 2 summarizes the metal content of the synthesised nanomaterials and their NP size, which were ascertained by inductively coupled plasma optical emission spectroscopy (ICP-OES) and transmission electron microscopy (TEM) analyses, respectively. Images of all the samples together with their respective size histograms are in displayed in the SI (Figures S4 to S6). Ru NP bearing the BINA(COOH)$_2$ ligand display similar NP size ranging from 1.6 to 2.2 nm. In the case of Ru/BINA(COOH)$_2$ series, the ICP are consistent among them displaying a metal content of *ca.* 70%.

Wide angle X-ray scattering (WAXS) analysis revealed well-crystallized Ru NP in the *hcp* structure ranging between 1 and 2.5 nm, confirming the TEM results, for the three tested samples, Ru/(*rac*)-BINA(COOH)$_2$, Ru/(*R*)-BINA(COOH)$_2$, and Ru/(*S*)-BINA(COOH)$_2$.The three samples show very similar WAXS pattern (Figure 2c) and d) and Figures S9–S11), so that a further simulation of the structure was only carried out on one of them (Ru/(*rac*)-BINA(COOH)$_2$). A fair agreement between the experimental pattern and the theoretical one, both on pair distribution function (PDF) and on reduced intensities (RI), was obtained using a mixture of two isotropic *hcp* model: 58 atoms (70%) with a diameter around 1.3 nm for the first one and 433 atoms (30%), d≈2.4 nm for the second model. This is consistent with the slight dual size distribution observed (Figure S4). However, a significantly better agreement was obtained using an anisotropic *hcp* model of 156 atoms measuring 0.9 nm along the a and b axes and 2,3 nm along the c axis. This may indicate that a fraction of the NP is elongated along the c axis with an elliptic shape.

Attenuated total reflection infrared (ATR-IR) spectra of Ru/BINA(COOH)$_2$ were recorded and compared to the spectra of the free ligand (Figure S12–S14). As similarly observed by some of us in previous works,[24,26] the characteristic C=O stretching band of the carboxylic acid appearing at 1685 cm^{-1} for BINA(COOH)$_2$ ligand, vanished after reaction, to give rise to several bands in the range of 1300–1750 cm^{-1}. A set of two

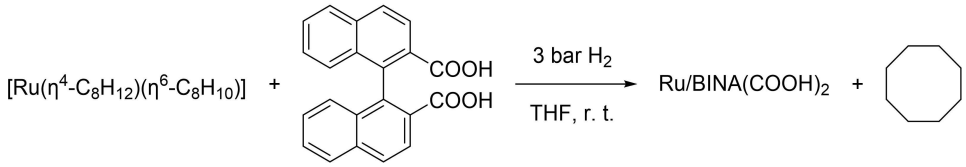

Scheme 2. Synthesis of Ru/BINA(COOH)$_2$.

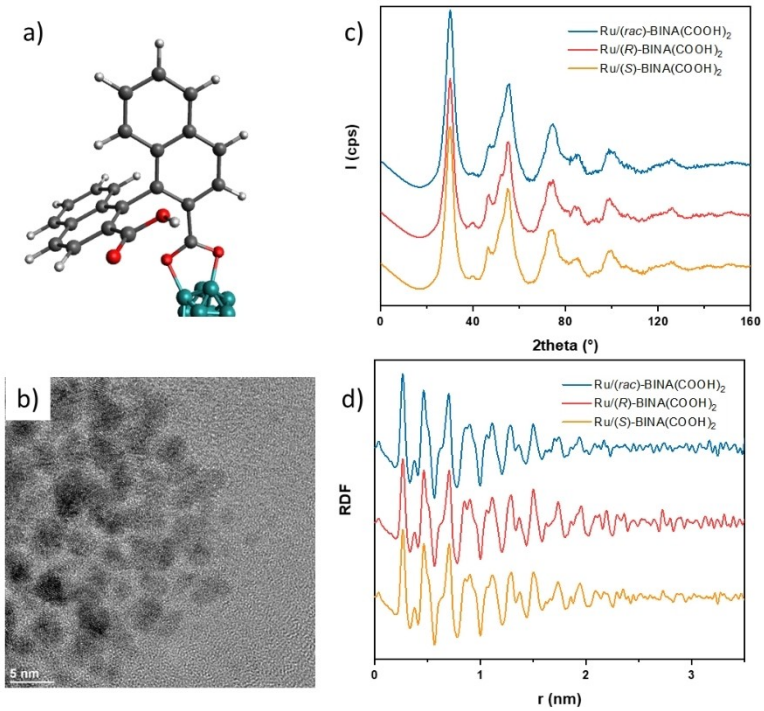

Figure 2. a) Schematic representation of the coordination of BINA(COOH)$_2$ onto a Ru NP surface; b) TEM image of Ru/(*rac*)-BINA(COOH)$_2$ (scale bar 5 nm); c) diffractograms of Ru/BINA(COOH)$_2$ series; and d) related radial distribution functions (RDFs).

Table 2. Metal content and mean size of metal nanoparticles.

NP	Ru content (%)[a]	Mean size (nm)[b]
Ru/(*rac*)-BINA(COOH)$_2$	70.2	1.6 ± 0.5
Ru/(*R*)-BINA(COOH)$_2$	60.0	1.9 ± 0.6
Ru/(*S*)-BINA(COOH)$_2$	70.3	2.2 ± 0.8
Ru/AdCOOH	41.6	1.9 ± 0.8
Ru/PVP	18.5	1.7 ± 0.4

[a] ICP analysis. [b] Mean values of nanoparticle size determined from TEM images by considering at least 200 particles.

bands, appearing at 1585 cm^{-1} and 1372 cm^{-1} with a $\Delta\nu \approx 200$ cm^{-1}, are consistent with bridging bidentate carboxylate ligands coordinated to the surface, *i.e.* both oxygens of the carboxylate moiety are coordinated to two different Ru atoms on the surface.[29] This coordination has been also observed for Ru/AdCOOH.[24] Nevertheless, in contrast to Ru/AdCOOH, a set of two bands, at 1724 cm^{-1} and 1352 cm^{-1} was attributed to the co-existence of free –COOH and/or monodentate coordination in the Ru/BINA(COOH)$_2$ nanomaterial.[26] Solid-state NMR (SS NMR) was performed on Ru/(*rac*)-BINA(COOH)$_2$ (Figure S15). ^{13}C SS NMR distinctly shows two sets of peaks, a peak at 136 ppm attributed to the binaphthyl moiety, and peak at 27 ppm, which was tentatively attributed to the presence of a partially reduced ligand. In addition, a broad low-intensity peak at 175 ppm is also observed, which was attributed to the C=O carbon of the carboxylate-ruthenium species together with free –COOH moieties.

As ascertained by the data summarized in Table 1, Ru colloidal catalysts were more active and selective towards 1-HQ in 1-PrOH. Accordingly, Ru/BINA(COOH)$_2$ series were used as catalysts in the hydrogenation of quinaldine using 1-PrOH as a solvent. Table 3 summarizes the catalytic performances of Ru/PVP, Ru/AdCOOH and Ru/BINA(COOH)$_2$ catalysts for this reaction, time-concentration curves of each reaction are given in SI (Figure S16 to S19). The addition of a carboxylic ligand to the NP surface increased considerably the TOF, effect more pronounced for Ru/AdCOOH. This catalyst displayed a TOF of 125 h^{-1} at 35 °C, which is in contrast with the one found for Ru/PVP, 22 h^{-1}. The electron density on the surface of the Ru nanocatalysts was estimated by measuring the ν_{CO} after CO exposure of the samples. Ru/PVP, Ru/AdCOOH, and Ru/BINA(COOH)$_2$ display a ν_{CO} of 2002, 1986, and 1990 cm^{-1}, respectively (Figure S21). The ν_{CO} correlated well with the measured TOF, lower CO frequency values, *i.e.* more electron density on the surface, displaying higher TOFs (Figure S21). In the case of the carboxylate stabilized Ru NP the ν_{CO} is similar, and the lower TOFs observed for Ru/BINA(COOH)$_2$ could be attributed to the more important steric hindrance of BINA(COOH)$_2$ with respect to the AdCOOH compound. In addition, the lower activity of Ru/BINA(COOH)$_2$ with respect to Ru/AdCOOH was accompanied with an increase of 1-HQ selectivity, from 68% (Ru/AdCOOH, Table 3, entry 8) to 81% (Ru/(*rac*)-BINA(COOH)$_2$, Table 3, entry 15), which is in line with the probable effect of the bulkiness of BINA(COOH)$_2$. Finally, the possible enantiomeric induction was measured in the final products by liquid chromatography, but in both cases, Ru/(*R*)-BINA(COOH)$_2$ or Ru/(*S*)-BINA(COOH)$_2$, no enantiomeric excess was observed.

All catalysts were analysed after the hydrogenation reaction by TEM (Figure S22–S36, Table S2). The sizes of the Ru NP after catalysis remain essentially the same than that of before catalysis. In the case of Ru/(*R*)-BINA(COOH)$_2$ and Ru/(*S*)-BINA(COOH)$_2$, the Ru content of the supernatant of the catalytic reaction was ascertained by ICP analyses. In both cases, traces of Ru were measured under the calibration limit, which correspond to less of 0.5% of Ru catalyst leaching. Both, TEM and ICP analyses pointing to a robust catalysts for this reaction. A filtration test was performed in a reaction performed with Ru/AdCOOH at r.t. under 35 bar of H_2 pressure; the catalyst was filtrated at partial conversion (1 h) through an alumina path and the clean solution reengaged for reaction under H_2 for 23 h. The reaction did not proceed after the filtration pointing to a heterogeneous catalysts operating (Figure S37). Four recycling tests were performed at partial conversion (1 h of reaction), ICP analyses were performed in each run on the solution, details are given in the experimental section. A loss of activity is observed from the first run (Figure S38), this may be attributed to several reasons, some leaching detected by ICP (less than 0.1% as in batch runs), the strong agglomeration of the Ru NP after 4 consecutive runs observed by TEM analyses (Figure S39), and the difficulty to fully separate the Ru NPs from 1-PrOH solution. On the other hand the Ru NP size remained comparatively similar than before catalysis (2.1 ± 0.4 *vs.* 1.9 ± 0.8 nm) as well as its crystal structure (Figure S39).

The possible interaction of quinaldine with the carboxylate present on the surface was examined by IR. Ru/AdCOOH was stirred in neat quinaldine at r.t. in a glovebox overnight, after that the excess of quinaldine was removed under vacuum at 80 °C, and the IR recorded. The IR spectra are presented in the SI (Figure S40). The IR spectrum did not show any significant difference with the untreated Ru/AdCOOH, thus pointing to a strong interaction of AdCOO- with the Ru surface. Further analyses are need though to understand the probably poisoning of intermediate compounds during the hydrogenation. Finally, the most active catalysts, Ru/AdCOOH, was tested in the hydrogenation of several quinoline related substrates. Results are summarized in Table 4.

1-HQ was not hydrogenated in these reaction conditions, pointing to a poisoning of the metallic surface, as discussed above. Similarly, 5-HQ was barely hydrogenated, 20%, probably for the same reason. Indole was barely hydrogenated in these conditions as well (Table 4, entry 8). Quinoline, Table 4, entry 4, was fully converted, very selectively, 91%, towards the N-bearing ring. A methyl in the carbocycle impeded the reduction on this aromatic ring (Table 4, entry 5). On the other hand, the addition of substituents on the N-ring enhanced the selectivity towards the carbocycle hydrogenation, reaching a selectivity towards it up to 66%. Thus, the nature and position of substituents play an important role in the selectivity of the

Table 3. Selective hydrogenation of quinaldine with Ru based nanocatalysts.[a]

Entry	T (°C)	t (h)	TOF (h^{-1})[b,c]	Conversion (%)[c]	1-HQ (%)[c]	5-HQ (%)[c]	HHQ (%)[c]
Ru/PVP							
1	r.t.[d]	1	6	4	61	27	12
2		3		19	63	28	9
3		24		97	52	26	22
4	35	1	22	13	58	33	9
5		3		49	55	33	12
6		24		>99	12	29	59
Ru/AdCOOH							
7	r.t.[d]	1	48	30	68	27	5
8		3		90	68	23	9
9		24		99	>1	20	79
10	35	1	125	69	66	22	12
11		3		99	54	19	26
12		24		>99	–	14	86
Ru/(*rac*)-BINA$(COOH)_2$							
13	r.t.[d]	1	14	9	85	12	3
14		3		33	88	10	2
15		24		99	81	8	11
16	35	1	82	53	77	15	8
17		3		99	68	14	18
18		24		>99	2	12	86
Ru/(*R*)-BINA$(COOH)_2$							
19	r.t.[d]	1	19	10	84	16	-
20		3		22	88	10	2
21		24		99	86	9	5
Ru/(*S*)-BINA$(COOH)_2$							
22	r.t.[d]	1	31	15	80	17	3
23		3		40	82	15	3
24		24		>99	77	12	11

[a] Reaction conditions: 3×10^{-2} mmol of metal, 3 mmol of quinaldine, 0.75 mmol of dodecane (internal standard), 35 bar of H_2, 15 mL of 1-PrOH. [b] TOFs calculated at 1 h of reaction according to the surface amount of metal. [c] Determined by GC using an internal standard technique. [d] Room temperature was in the range 20–23 °C.

reaction, also, it seems to emerge that the Lewis-basicity is playing a role on the outcome of the reaction.

Conclusions

The hydrogenation towards the N-bearing cycle of quinaldine was enhanced in polar solvents; non-polar solvents led to lower activities but with a preference for the hydrogenation of the carbocycle, reaching selectivities up to 70% at full conversion using Ru/AdCOOH in Et_2O. Having demonstrated that the presence of carboxylate ligands at the Ru NP surface enhances activity and selectivity towards the hydrogenation of the N-containing cycle a series of Ru NP ligands containing a bulky chiral backbone were synthesised in an attempt to achieve chiral induction in the hydrogenated quinaldine. The nanocatalysts were remarkably active at low temperature for the hydrogenation of quinaldine, giving full conversion after 24 h of reaction in 1-PrOH with a selectivity towards the partially hydrogenated 1-HQ product of 86%. Unfortunately, no enantiomeric excess was observed.

Experimental section

General methods. All operations were carried out under argon atmosphere using standard Schlenk techniques or in an MBraun glovebox. Solvents were purified by standard methods or by an MBraun SPS-800 solvent purification system. [Ru(η^4-C_8H_{12})(η^6-C_8H_{10})] was purchased from Nanomeps Toulouse, (R)-, (S)- and (racemic)-1,1′-binaphthalene-2,2′-dicarboxylic acid were prepared following a modified procedure described elsewhere,[44] quinaldine, 1-HQ, 5-HQ and HHQ from TCI, solvents and AdCOOH from Aldrich, CO and H_2

Table 4. Selective hydrogenation of quinoline derivatives with Ru/AdCOOH nanocatalyst.[a]

Entry	Substrate	Conversion (%)[c]	1-HQ (%)[c]	5-HQ (%)[c]	HHQ (%)[c]
1	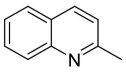	>99	21	18	61
2[b]	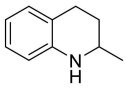	–	–	–	–
3[b]	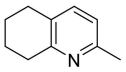	20	–	–	>99
4	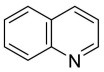	>99	91	6	3
5	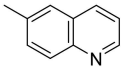	>99	72	–	28
6	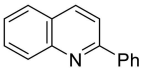	73	16	66	18*
7	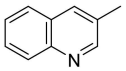	89	34	62	3
8		3	–	100	–

[a] Reaction conditions: 1×10^{-2} mmol of metal, 1 mmol of substrate, 0.25 mmol of dodecane (internal standard), 35 bar of H_2, 5 mL of 1-PrOH, room temperature (20–23 °C). [b] Reaction conditions: 3×10^{-2} mmol of metal, 3 mmol of 1-HQ or 5-HQ, 0.75 mmol of dodecane (internal standard), 35 bar of H_2, 15 mL of 1-PrOH, room temperature (20–23 °C). [c] Determined by GC using an internal standard technique.*including four phenyl hydrogenated products, as determined by GCMS.

from Air Liquid. All these reactants were used as received. Metal content was established by ICP-OES performed in a Thermo Scientific ICAP 6300 instrument. Elemental analyses were performed in a PERKIN ELMER 2400 serie II analyzer. Liquid NMR measurements were performed on a Bruker Avance 300 or 400 instrument. ATR-IR spectra were recorded on a Perkin-Elmer GX2000 spectrometer available in a glovebox, in the range 4000–400 cm^{-1}. TEM analyses were performed at the "Centre de microcaracterisation Raimond Castaing, UAR 3623, Toulouse" by using a JEOL JEM 1011 electron microscope operating at 100 kV with a point resolution of 4.5 Å, a JEOL JEM 1400 operating at 120 kV with a point resolution of 2.0 Å, or a JEOL JEM 2100F – EDS operating at 200 kV with a point resolution of 2.3 Å. The approximation of the particles mean size was stablished through a manual analysis of enlarged micrographs by measuring at least 200 particles on a given grid. WAXS measurements were performed at CEMES on a diffractometer dedicated to Pair Distribution Function (PDF) analysis: graphite-monochromatized Molybdenum radiation (0.07169 nm), solid-state detection and low background setup. Samples were sealed in Lindemann glass capillaries (diameter 1 mm) to avoid any oxidation after filling them in a glove box. For all samples data were collected on an extended angular range (129 degrees in 2theta) with counting times of typically 150s for each of the 457 data points, thus allowing for PDF analysis. Classic corrections (polarization and absorption in cylindrical geometry) were applied before reduction and Fourier transform. Quantitative analyses of the catalytic reaction mixtures were performed via GC analyses using internal standard technique and solutions of commercially available products. GC analyses were performed on a SHIMADZU GC-2014 equipped with a SUPELCOWAX 10 capillary column (30 m×0.25 mm×0.25 μm). The method used for quinaldine reaction mixture analyses consists on: carrier gas flow, He, 1.25 ml/min; injector temperature, 250 °C; detector (FID) temperature, 250 °C; oven program, 50 °C, hold for 3 min, to 240 °C at 20 °C/min, hold for 10 min for a total run time of 22.5 min; retention time: dodecane, 6.8 min; HHQ, 8.5 and 8.8 min, 5-THQ, 11.1 min; quinaldine, 12.3 min; and 1-THQ, 12.5 min. Enantiomeric excess of the 1-HQ product was measured at SPCMIB-Tolouse by chiral stationary phase HPLC analysis using Chiralcel OJ–H 5 μm 4.6x250 mm (heptane: i–PrOH 9:1 at 0.5 mL/min): $tS = 19.0$ min, $tR = 20.6$ min.[45]

Synthesis of Ru NP. In a typical experiment, $[Ru(\eta^4\text{-}C_8H_{12})(\eta^6\text{-}C_8H_{10})]$ complex was introduced in a Fisher Porter bottle, together with the corresponding dicarboxylic acid ligand, 1-adamantanecarboxylic acid, or PVP, and then dissolved with THF in a glovebox. The yellow solution was then pressurized with 3 bar of H_2 at room temperature. After some minutes, the solution turned black. The reaction was kept overnight under vigorous stirring. After this period of time, the H_2 excess was removed and pentane was added to precipitate the NP. After filtration under argon with a cannula, the black solid powder was washed twice with pentane and filtered again before drying under reduced pressure overnight. For each ratio studied, the quantities of reactants are detailed hereafter. % are in weight.

Ru/PVP: 150 mg (0.476 mmol) of $[Ru(\eta^4\text{-}C_8H_{12})(\eta^6\text{-}C_8H_{10})]$, 140 mg of PVP, and 40 mL of THF. Yield: 163.0 mg. ICP anal.: 18.5 % Ru.

Ru/AdCOOH: 300 mg (0.951 mmol) of $[Ru(\eta^4\text{-}C_8H_{12})(\eta^6\text{-}C_8H_{10})]$, 34 mg (0.096 mmol) of AdCOOH, and 25 mL of THF. Yield: 71.8 mg. Anal.: 41.6 % Ru.

Ru/(*R*)-BINA(COOH)$_2$: 300 mg (0.951 mmol) of [Ru(η^4-C_8H_{12})(η^6-C_8H_{10})], 33 mg (0.096 mmol) of (*R*)-1,1′-binaphthalene-2,2′-dicarboxylic acid, and 25 mL of THF. Yield: 105.3 mg. Anal.: 60.0 % Ru, 18.74 %C, 0.96 % H.

Ru/(*S*)-BINA(COOH)$_2$: 300 mg (0.951 mmol) of [Ru(η^4-C_8H_{12})(η^6-C_8H_{10})], 33 mg (0.096 mmol) of (*S*)-1,1′-binaphthalene-2,2′-dicarboxylic acid, and 25 mL of THF. Yield: 129.4 mg. Anal.: 70.3 % Ru, 18.86 %C, 0.86 % H.

Ru/(*rac*)-BINA(COOH)$_2$: 300 mg (0.951 mmol) of [Ru(η^4-C_8H_{12})(η^6-C_8H_{10})], 33 mg (0.096 mmol) of (*racemic*)-1,1′-binaphthalene-2,2′-dicarboxylic acid, and 25 mL of THF. Yield: 129.4 mg. Anal.: 70.2 % Ru, 16.89 %C, 0.41 % H.

Surface reactivity with CO. The adsorption of CO on the surface of the nanostructures was performed in the solid state as follows: A purified sample of NP was introduced in a Fischer-Porter bottle. The reactor was pressurized with 1.5 bar of CO for 24 h. Then, the CO gas was evacuated under reduced pressure for 20 min, and the ATR-IR spectra recorded in a glovebox.

Surface reactivity with quinaldine. Ru/AdCOOH, 5 mg, was dispersed in 0,5 mL of quinaldine and stirred overnight at r.t. under Ar. Quinaldine was then removed under vacuum at 80 °C. After that, he ATR-IR spectra of the black solid was recorded in a glovebox.

Catalytic hydrogenations. The hydrogenation of quinaldine was carried out in a 50 mL stainless steel high-pressure batch Top Industrie reactor. In a typical batch experiment, a mixture of the catalyst (0.01 mmol of metal), dodecane (0.25 mmol) as internal standard, and quinaldine (1 mmol) or the desired substrate in 5 mL of the desired solvent were loaded into the autoclave in the glovebox. The autoclave was purged three times with H_2 to remove the inert atmosphere, heated to the desired temperature, and charged with 35 bar of H_2. The stirring rate was fixed at 1200 rpm. For the filtration test, the reaction was depressurized after 1 h of reaction at r.t., the reaction mixture was filtered through an alumina path and the clean solution pressurized again with 35 bar of H_2 and allowed to react for 23 h more. In the case that samples of the reaction mixture were taken at different time intervals the procedure was the same but using a mixture of the catalyst (0.03 mmol of metal), dodecane (0.75 mmol) as internal standard, and quinaldine (3 mmol) as substrate in 15 mL of 1-PrOH. For the recycling test, the first reaction was performed as described above; after 1 h of reaction the reactor was depressurized and introduced into the GB; the catalyst was allowed to precipitate overnight, and the solution was cannuled for GC and ICP analyses; the recycled catalyst was engaged in a new reaction with dodecane (0.75 mmol) as internal standard, quinaldine (3 mmol) and 15 mL of 1-PrOH; the procedure was repeated for four cycles. Samples of the reactions were analysed by gas chromatography. Quantitative analyses of the reaction mixtures were performed via GC using calibration solutions of commercially available products.

Author Contributions

V. C. performed the TEM analyses. M. V. and P. L. performed the WAXS analyses and interpreted the results. M. R. A. synthesized and participated in the characterization of the catalysts, performed the catalytic studies, conceived and coordinated this work.

Acknowledgements

This work was supported by the CNRS, which we gratefully acknowledge.

Conflict of Interests

The authors declare no conflict of interest.

Data Availability Statement

The data that support the findings of this study are available in the supplementary material of this article.

Keywords: selective arene hydrogenation · ruthenium · nanoparticles · chemoselectivity · heterocycles

[1] M. P. Wiesenfeldt, Z. Nairoukh, T. Dalton, F. Glorius, *Angew. Chem. Int. Ed.* **2019**, *58*, 10460–10476.
[2] W. C. Wertjes, E. H. Southgate, D. Sarlah, *Chem. Soc. Rev.* **2018**, *47*, 7996–8017.
[3] a) W.-B. Wang, S.-M. Lu, P.-Y. Yang, X.-W. Han, Y.-G. Zhou, *J. Am. Chem. Soc.* **2003**, *125*, 10536–10537; b) E. R. Welin, A. Ngamnithiporn, M. Klatte, G. Lapointe, G. M. Pototschnig, M. S. J. McDermott, D. Conklin, C. D. Gilmore, P. M. Tadross, C. K. Haley, K. Negoro, E. Glibstrup, C. U. Gruenanger, K. M. Allan, S. C. Virgil, D. J. Slamon, B. M. Stoltz, *Science* **2019**, *363*, 270–275; c) Z. Nairoukh, M. Wollenburg, C. Schlepphorst, K. Bergander, F. Glorius, *Nat. Chem.* **2019**, *11*, 264–270; d) B. Qu, H. P. R. Mangunuru, S. Tcyrulnikov, D. Rivalti, O. V. Zatolochnaya, D. Kurouski, S. Radomkit, S. Biswas, S. Karyakarte, K. R. Fandrick, J. D. Sieber, S. Rodriguez, J.-N. Desrosiers, N. Haddad, K. McKellop, S. Pennino, H. Lee, N. K. Yee, J. J. Song, M. C. Kozlowski, C. H. Senanayake, *Org. Lett.* **2018**, *20*, 1333–1337; e) X. Wei, B. Qu, X. Zeng, J. Savoie, K. R. Fandrick, J.-N. Desrosiers, S. Tcyrulnikov, M. A. Marsini, F. G. Buono, Z. Li, B.-S. Yang, W. Tang, N. Haddad, O. Gutierrez, J. Wang, H. Lee, S. Ma, S. Campbell, J. C. Lorenz, M. Eckhardt, F. Himmelsbach, S. Peters, N. D. Patel, Z. Tan, N. K. Yee, J. J. Song, F. Roschangar, M. C. Kozlowski, C. H. Senanayake, *J. Am. Chem. Soc.* **2016**, *138*, 15473–15481.
[4] I. Muthukrishnan, V. Sridharan, J. C. Menendez, *Chem. Rev.* **2019**, *119*, 5057–5191.
[5] D. Ren, L. He, L. Yu, R.-S. Ding, Y.-M. Liu, Y. Cao, H.-Y. He, K.-N. Fan, *J. Am. Chem. Soc.* **2012**, *134*, 17592–17598.
[6] a) D. Ge, L. Hu, J. Wang, X. Li, F. Qi, J. Lu, X. Cao, H. Gu, *ChemCatChem* **2013**, *5*, 2183–2186; b) S. Zhang, Z. Xia, T. Ni, Z. Zhang, Y. Ma, Y. Qu, *J. Catal.* **2018**, *359*, 101–111.
[7] M. Guo, C. Li, Q. Yang, *Catal. Sci. Technol.* **2017**, *7*, 2221–2227.
[8] Y.-G. Ji, K. Wei, T. Liu, L. Wu, W.-H. Zhang, *Adv. Synth. Catal.* **2017**, *359*, 933–940.
[9] Z. Luo, Y. Min, D. Nechiyil, W. Bacsa, Y. Tison, H. Martinez, P. Lecante, I. C. Gerber, P. Serp, M. R. Axet, *Catal. Sci. Technol.* **2019**, *9*, 6884–6898.
[10] M. Mateen, K. Shah, Z. Chen, C. Chen, Y. Li, *Nano Res.* **2019**, *12*, 1631–1634.
[11] D. J. M. Snelders, N. Yan, W. Gan, G. Laurenczy, P. J. Dyson, *ACS Catal.* **2012**, *2*, 201–207.
[12] X. Cui, A.-E. Surkus, K. Junge, C. Topf, J. Radnik, C. Kreyenschulte, M. Beller, *Nat. Commun.* **2016**, *7*, 11326pp.
[13] B. Sun, D. Carnevale, G. Suss-Fink, *J. Organomet. Chem.* **2016**, *821*, 197–205.
[14] a) Y. Chen, Z. Yu, Z. Chen, R. Shen, Y. Wang, X. Cao, Q. Peng, Y. Li, *Nano Res.* **2016**, *9*, 2632–2640; b) A. A. Alharbi, C. Wills, T. W. Chamberlain, R. A. Bourne, A. Griffiths, S. M. Collins, K. Wu, P. Mueller, J. G. Knight, S. Doherty, *ChemCatChem* **2023**, *15*, e202300418.
[15] B. Sahoo, C. Kreyenschulte, G. Agostini, H. Lund, S. Bachmann, M. Scalone, K. Junge, M. Beller, *Chem. Sci.* **2018**, *9*, 8134–8141.
[16] a) F. Chen, A.-E. Surkus, L. He, M.-M. Pohl, J. Radnik, C. Topf, K. Junge, M. Beller, *J. Am. Chem. Soc.* **2015**, *137*, 11718–11724; b) K. Murugesan, V. G.

Chandrashekhar, C. Kreyenschulte, M. Beller, R. V. Jagadeesh, *Angew. Chem. Int. Ed.* **2020**, *59*, 17408–17412; c) I. Sorribes, L. Liu, A. Domenech-Carbo, A. Corma, *ACS Catal.* **2018**, *8*, 4545–4557; d) J. Li, G. Liu, X. Long, G. Gao, J. Wu, F. Li, *J. Catal.* **2017**, *355*, 53–62; e) Z. Wei, Y. Chen, J. Wang, D. Su, M. Tang, S. Mao, Y. Wang, *ACS Catal.* **2016**, *6*, 5816–5822; f) M. Puche, L. Liu, P. Concepcion, I. Sorribes, A. Corma, *ACS Catal.* **2021**, *11*, 8197–8210; g) C. Bauer, F. Mueller, S. Keskin, M. Zobel, R. Kempe, *Chem. Eur. J.* **2023**, *29*, e202300561.

[17] C. Liu, Z. Rong, Z. Sun, Y. Wang, W. Du, Y. Wang, L. Lu, *RSC Adv.* **2013**, *3*, 23984–23988.

[18] V. Papa, Y. Cao, A. Spannenberg, K. Junge, M. Beller, *Nat. Catal.* **2020**, *3*, 135–142.

[19] a) Y.-G. Zhou, *Acc. Chem. Res.* **2007**, *40*, 1357–1366; b) A. N. Kim, B. M. Stoltz, *ACS Catal.* **2020**, *10*, 13834–13851.

[20] J. Pérez-Ramírez, N. López, *Nat. Catal.* **2019**, *2*, 971–976.

[21] a) M. A. Ortuno, N. Lopez, *Catal. Sci. Technol.* **2019**, *9*, 5173–5185; b) L. Lu, S. Zou, B. Fang, *ACS Catal.* **2021**, *11*, 6020–6058.

[22] a) D. Krishnan, L. Schill, M. R. Axet, K. Philippot, A. Riisager, *Nanomaterials* **2023**, accepted; b) L. Bruna, M. Cardona-Farreny, V. Colliere, K. Philippot, M. R. Axet, *Nanomaterials* **2022**, *12*, 328.

[23] M. R. Axet, S. Conejero, I. C. Gerber, *ACS Appl. Nano Mater.* **2018**, *1*, 5885–5894.

[24] Y. Min, H. Nasrallah, D. Poinsot, P. Lecante, Y. Tison, H. Martinez, P. Roblin, A. Falqui, R. Poteau, I. del Rosal, I. C. Gerber, J.-C. Hierso, M. R. Axet, P. Serp, *Chem. Mater.* **2020**, *32*, 2365–2378.

[25] Y. Min, F. Leng, B. F. Machado, P. Lecante, P. Roblin, H. Martinez, T. Theussl, A. Casu, A. Falqui, M. Barcenilla, S. Coco, B. M. I. Martinez, N. Martin, M. R. Axet, P. Serp, *Eur. J. Inorg. Chem.* **2020**, *2020*, 4069–4082.

[26] F. Leng, I. C. Gerber, P. Lecante, A. Bentaleb, A. Munoz, B. M. Illescas, N. Martin, G. Melinte, O. Ersen, H. Martinez, M. R. Axet, P. Serp, *Chem. Eur. J.* **2017**, *23*, 13379–13386.

[27] F. Leng, I. C. Gerber, P. Lecante, S. Moldovan, M. Girleanu, M. R. Axet, P. Serp, *ACS Catal.* **2016**, *6*, 6018–6024.

[28] L. Cusinato, L. M. Martinez-Prieto, B. Chaudret, I. del Rosal, R. Poteau, *Nanoscale* **2016**, *8*, 10974–10992.

[29] R. Gonzalez-Gomez, L. Cusinato, C. Bijani, Y. Coppel, P. Lecante, C. Amiens, I. del Rosal, K. Philippot, R. Poteau, *Nanoscale* **2019**, *11*, 9392–9409.

[30] W. M. Haynes, Editor, *CRC Handbook of Chemistry and Physics, 95th Edition*, CRC Press, **2014**.

[31] a) C. L. Young, Editor, *Solubility data series, Vol. 5/6: hydrogen and deuterium*, **1981**; b) E. Brunner, *J. Chem. Eng. Data* **1985**, *30*, 269–273; c) T.-K.-H. Trinh, J.-C. de Hemptinne, R. Lugo, N. Ferrando, J.-P. Passarello, *J. Chem. Eng. Data* **2016**, *61*, 19–34.

[32] C. Chaudhari, H. Imatome, Y. Nishida, K. Sato, K. Nagaoka, *Catal. Commun.* **2019**, *126*, 55–60.

[33] L. Petitjean, R. Gagne, E. S. Beach, J. An, P. T. Anastas, D. Xiao, *ACS Sustainable Chem. Eng.* **2017**, *5*, 10371–10378.

[34] B. Chan, L. Radom, *J. Am. Chem. Soc.* **2005**, *127*, 2443–2454.

[35] a) R. P. K. Wells, N. R. McGuire, X. Li, R. L. Jenkins, P. J. Collier, R. Whyman, G. J. Hutchings, *Phys. Chem. Chem. Phys.* **2002**, *4*, 2839–2845; b) B.-J. Liu, T. Torimoto, H. Matsumoto, H. Yoneyama, *J. Photochem. Photobiol. A* **1997**, *108*, 187–192; c) L. Nikoshvili, E. Shimanskaya, A. Bykov, I. Yuranov, L. Kiwi-Minsker, E. Sulman, *Catal. Today* **2015**, *241*, 179–188.

[36] N. Yan, J.-G. Zhang, Y. Tong, S. Yao, C. Xiao, Z. Li, Y. Kou, *Chem. Commun.* **2009**, *45*, 4423–4425.

[37] a) A. F. Borowski, S. Sabo-Etienne, B. Donnadieu, B. Chaudret, *Organometallics* **2003**, *22*, 1630–1637; b) A. F. Borowski, L. Vendier, S. Sabo-Etienne, E. Rozycka-Sokolowska, A. V. Gaudyn, *Dalton Trans.* **2012**, *41*, 14117–14125; c) S. Urban, N. Ortega, F. Glorius, *Angew. Chem. Int. Ed.* **2011**, *50*, 3803–3806; d) R. Kuwano, R. Ikeda, K. Hirasada, *Chem. Commun.* **2015**, *51*, 7558–7561; e) Y. Jin, Y. Makida, T. Uchida, R. Kuwano, *J. Org. Chem.* **2018**, *83*, 3829–3839.

[38] a) M. Hoenel, F. W. Vierhapper, *J. Chem. Soc. Perkin Trans. 1* **1982**, 2607–2610; b) M. Hoenel, F. W. Vierhapper, *J. Chem. Soc. Perkin Trans. 1* **1980**, 1933–1939; c) F. W. Vierhapper, E. L. Eliel, *J. Org. Chem.* **1975**, *40*, 2729–2734; d) A. Solladie-Cavallo, M. Roje, A. Baram, V. Sunjic, *Tetrahedron Lett.* **2003**, *44*, 8501–8503; e) K. A. Skupinska, E. J. McEachern, R. T. Skerlj, G. J. Bridger, *J. Org. Chem.* **2002**, *67*, 7890–7893.

[39] a) H. Konnerth, M. H. G. Prechtl, *Green Chem.* **2017**, *19*, 2762–2767; b) H.-Y. Jiang, X.-X. Zheng, *Catal. Sci. Technol.* **2015**, *5*, 3728–3734; c) A. Kumar, V. Goyal, N. Sarki, B. Singh, A. Ray, T. Bhaskar, A. Bordoloi, A. Narani, K. Natte, *ACS Sustainable Chem. Eng.* **2020**, *8*, 15740–15754.

[40] S. Zhang, J. Xu, H. Cheng, C. Zang, B. Sun, H. Jiang, F. Bian, *Appl. Catal. A* **2020**, *596*, 117536.

[41] a) F. Meemken, A. Baiker, *Chem. Rev.* **2017**, *117*, 11522–11569; b) M. Heitbaum, F. Glorius, I. Escher, *Angew. Chem. Int. Ed.* **2006**, *45*, 4732–4762; c) K. Ding, Y. Uozumi, Editors, *Handbook of asymmetric heterogeneous catalysis*, **2008**.

[42] a) T. Sugimura, *Heterogeneous enantioselective hydrogenation on metal surface modified by chiral molecules*, (Eds.: K. Ding, Y. Uozumi), **2008**, pp. 357–382; b) L. Hadian-Dehkordi, H. Hosseini-Monfared, *Green Chem.* **2016**, *18*, 497–507.

[43] a) C. Bianchini, P. Barbaro, G. Scapacci, E. Farnetti, M. Graziani, *Organometallics* **1998**, *17*, 3308–3310; b) D.-S. Wang, Q.-A. Chen, S.-M. Lu, Y.-G. Zhou, *Chem. Rev.* **2012**, *112*, 2557–2590; c) L. Shi, Y.-G. Zhou, *Org. React.* **2018**, *96*, 1–227.

[44] L. Zhao, D. Qi, K. Wang, T. Wang, B. Han, Z. Tang, J. Jiang, *Sci. Rep.* **2016**, *6*, 28026pp.

[45] H. Zhou, Z. Li, Z. Wang, T. Wang, L. Xu, Y. He, Q.-H. Fan, J. Pan, L. Gu, A. S. C. Chan, *Angew. Chem. Int. Ed.* **2008**, *47*, 8464–8467.

Manuscript received: July 4, 2023
Accepted manuscript online: December 22, 2023
Version of record online: ■■, ■■

RESEARCH ARTICLE

Colloidal ruthenium nanoparticles are selective catalysts for heterocycle hydrogenations at room temperature. Control over activity and chemoselectivity are achieved by both changing the reaction solvent and the stabilizing ligands. The hydrogenation of the carbocycle is attained with a selectivity up to 70% at full conversion.

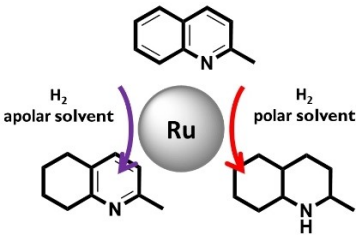

*V. Colliere, Dr. M. Verelst, Dr. P. Lecante, Dr. M. R. Axet**